Complex Waveguide Supermode Analysis of Coherently-Coupled Microcavity Laser Arrays

Pawel Strzebonski and Kent D. Choquette, *Fellow, IEEE*

***Abstract*—Coherently coupled microcavity lasers have desirable properties for emerging applications. We use 2-dimensional complex refractive index waveguide modeling of 2-element photonic crystal vertical cavity surface emitting laser arrays to analyze their supermodes. The complex modal effective indices are used in turn to calculate the complex coupling coefficient between the laser array elements. An analysis of the effects of array design parameters, such as photonic crystal period, fill-factor, or confinement, to engineer the coupling coefficient for the desired properties is given and example designs for 850 nm arrays are presented.**

***Index Terms*—Laser modes, optical coupling, phased arrays, semiconductor laser arrays, vertical-cavity surface emitting lasers (VCSEL).**

I. Introduction

COHERENTLY coupled 2-element arrays of photonic crystal vertical cavity surface emitting lasers (VCSELs) have been shown to exhibit novel dynamic properties such as increased small-signal modulation bandwidth [1], [2], enhanced digital data transmission [3], and reduced intensity noise and harmonic distortion [4]. When coherently coupled, the photonic crystal VCSEL arrays emit into non-Hermitian supermodes [5] that exhibit beam steering [6] and exceptional points [7]. The enhancements to the modulation performance are attributed to photon-photon resonance effects [3], driven by the field beating of array supermodes.

Coherently coupled arrays of lasers, whether VCSELs [8] or distributed feedback lasers [9], are often characterized by a coupling coefficient that quantifies the coupling between the optical fields in the individual cavities. The coupling coefficient has been calculated using a variety of different methods, including analytical analysis of coupled mode equations [10] or perturbation-based methods [11]. Supermode analysis of arrays of identical waveguides has linked the coupling coefficients to the difference in the modal propagation constants of the array supermodes [12]. This provides an intuitive link between the array waveguide structure and supermodes, and the coupling coefficient and the photon-photon resonance effects that it describes.

Manuscript received March 31, 2021; revised May 23, 2021; accepted July 5, 2021. Date of publication July 9, 2021; date of current version August 3, 2021. *(Corresponding author: Pawel Strzebonski.)*

The authors are with the Electrical and Computer Engineering Department, University of Illinois, Urbana, IL 61801 USA (e-mail: strzebo2@illinois.edu; choquett@illinois.edu).

Color versions of one or more figures in this article are available at https://doi.org/10.1109/JSTQE.2021.3096167.

Digital Object Identifier 10.1109/JSTQE.2021.3096167

The effect of waveguide design parameters (in the context of arrays of VCSELs) on the coupling coefficent has been previously studied using analytical methods [10] as well as numerical array supermode analysis [13]. However, these past analyses have been limited in the scope of VCSEL array design parameters that can be effectively evaluated, due to either difficulty in analytically modeling some parameters or the use of 1-dimensional (1D) effective waveguide structures. We build on past numerical supermode analysis by extending it to 2-dimensional (2D) complex refractive index structures. Two dimensional models are a more accurate simulation of physical structures and design parameters, and the use of complex refractive index enables the calculation of complex coupling coefficients. The imaginary part of the coupling coefficient represents the gain difference between the elements, which dictates which of the nearly degenerate supermodes is dominant [5]. We recently reported a technique to experimentally measure both the real and imaginary components of the coupling coefficient using simultaneous measurements of output power, near-field intensity, and far-field profile [14], [15]. In this work we will focus on a 2D waveguide model corresponding to 2×1 photonic crystal VCSEL array structures and evaluate the effects of a few key design parameters on the complex coupling coefficient.

II. Theory and Methods

A. Modes, Coupling, and Photon-Photon Resonance

Coherently coupled operation in VCSEL arrays occurs when the individual laser cavities do not operate with their fields confined to an individual cavity, but rather a coherent optical supermode whose field spans across multiple cavities. However, rate equation and modulation analysis of coherently coupled VCSEL arrays model such systems as individual cavities with their own carrier and photon reservoirs, the latter being linked via a coupling coefficient, κ [16], [17]. This coupling coefficient can be derived from array supermode analysis, as the coupling coefficient is proportional to the difference in the propagation constants for a pair of array supermodes [13].

The array supermodes can be characterized by a modal field and a modal effective index, n_{eff}. The modal effective index is related to the mode propagation constant [18]

$$\beta = \frac{2\pi n_{\text{eff}}}{\lambda_0} \tag{1}$$

where λ_0 is the free-space wavelength for the mode. In the simple case of an array of two identical waveguides the coupling

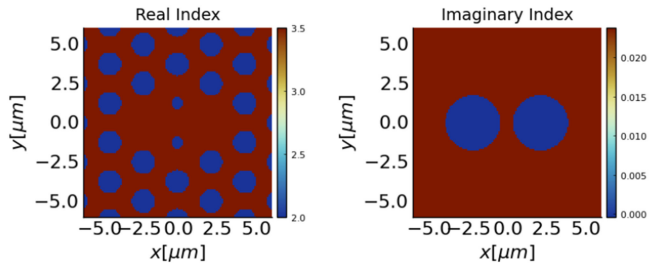

Fig. 1. Refractive index structure for a waveguide model for a typical 2×1 array of photonic crystal VCSELs.

TABLE I
DESIGN/SIMULATION PARAMETERS FOR FIG. 1 AND CORRESPONDING SIMULATIONS. THE PERIOD VARIES BETWEEN 2-3 μm AND PITCH BETWEEN 0.5-0.7

Parameter:	Symbol:	Value:
Wavelength	λ_0	850 nanometers
Bulk index	n_{bulk}	$3.5 + 0.02378i$
Index suppression	Δn or $n_{\text{suppression}}$	0.005
Cavity gain	k	~ 0.0004302
Core index	n_{core}	$3.495 - 0.0004302i$
Hole index	n_{hole}	$2 + 0.02378i$
PhC period	Λ	2.5 μm
PhC fill-factor	FF	0.6

coefficient can be simply derived from the difference in the propagation constants of the array supermodes. Throughout this work all of the waveguide models are composed of two identical waveguides. The coupling coefficient (in spatial units) for a pair of modes is [13]:

$$\kappa_{\text{spatial}} = \frac{\Delta\beta}{2} = \frac{\pi \Delta n_{\text{eff}}}{\lambda_0} \tag{2}$$

The photon-photon resonance frequency is related to the beating between the modal fields and can be related to the coupling coefficient. The coupling coefficient in temporal units [14]

$$\kappa_{\text{temporal}} = v_g \kappa_{\text{spatial}} \approx v_p \kappa_{\text{spatial}} \tag{3}$$

where v_g and v_p are the group and phase velocities. As the modal effective indices can be complex (in the case of waveguides with loss or gain), the propagation constant and coupling coefficients can be likewise complex.

B. Photonic Crystal VCSEL Array Model and Mode-Solving

The photonic crystal VCSEL arrays studied here have two laser cavities which are defined by missing-hole defects in a triangular lattice of etched holes introduced in the top distributed Bragg reflector (DBR) mirror. The etched photonic crystal holes provide transverse optical confinement, while electrical confinement is provided by a ion-implant aperture within the missing-hole defect region. Arrays of cavities are created by multiple adjacent missing-hole defects (not along a lattice axis, but rather along the direction between two lattice axes), and by shrinking the holes between the cavities (these shrunk holes have radii reduced to half of the regular hole radius) [2]. The injection aperture is assumed to be the circle that is tangent to the surrounding etched holes The 2-element array that is analyzed is illustrated in Fig. 1.

For modeling the VCSEL arrays as 2D waveguides, we start by determining the refractive index values for our model. At a wavelength of 850 nanometers undoped GaAs has a complex index $n \approx 3.5708 + 0.02426i$ [19]. However, our structure is a GaAs/AlGaAs cavity defined by a pair of doped DBR mirrors which would imply a lower real index value (as AlGaAs has a lower index than GaAs) and higher imaginary component (as higher carrier concentrations would increase free-carrier absorption). Past work using a simplified cylindrical step-index optical fiber waveguide model for a single cavity has assumed a real index value of 3.5 and would use a cladding imaginary index value of 0.05 to model all of the losses in the cladding layers [20] (this value incorporates all losses, both material and photonic crystal effects). We assume that the same real index value of 3.5 from [20] but will use an imaginary index value estimated from [19]. We correspondingly scale down the complex index of GaAs for an assumed bulk complex index value of $n \approx 3.5 + 0.02378i$ (assuming that additional losses due to doping are negligible and that the effect of the AlGaAs layers decreases the imaginary index in proportion to the real index). The photonic crystal etch regions will have lowered effective refractive index in our model as part of the DBR stack is replaced by air. We assume that the real component of index is 2 and that the imaginary component remains the same for a complex etch-hole index value of $n \approx 2 + 0.02378i$. Under injection, the laser cavity (defined by the ion implant aperture) will be index antiguiding with an index suppression that is estimated to be $\Delta n = 0.005$ relative to the bulk index value due to carrier-dependent index-shift effects [21]. Furthermore, the injection produces gain. We estimate the gain coefficient using typical values of the mirror and internal loss coefficients [18] as approximately 63.6 cm^{-1} giving a complex core index of $n \approx 3.495 - 0.0004302$.

Having defined a 2D waveguide index structure (key design parameters are summarized in Table I), we proceed to solve for the array modes (for a free-space wavelength of 850 nanometers) using a finite difference method solver of the scalar Helmholtz waveguide equation [18]. For index-confined laser cavities, solving for the modal effective index allows determination of the threshold mode. However, for anti-guided laser cavities, it is appropriate to rank the modes based on their confinement factor (fraction of modal power contained within the cavity) [22]. Thus for the antiguided supermodes, it is important to solve for a greater number of modes (including both bound and unbound modes) and select the modes whose confinement factor shows a significant portion of the modal power within the cavity [13], [22]. In addition, expanding the simulation domain to include more periods of the photonic crystal improves the mode-solver convergence to the confined modes. In Fig. 2(a) we plot the modal confinement factor Γ for the first 20 modes, as well as the modal effective indices in Fig. 2(b). While the first two modes (by real modal effective index) have very high confinement factor in Fig. 2(a), the next couple modes have negligible confinement and Fig. 2(b) shows they also have large imaginary index compenent indicating spurious mode solutions.

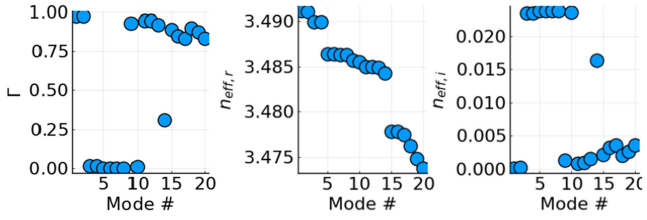

(a) Modal confinement factors (b) Modal effective indices

Fig. 2. Mode simulation results for a typical 2×1 array of photonic crystal VCSELs (waveguide structure illustrated in Fig. 1).

Once the waveguide supermodes are found (along with their modal effective indices), the two supermodes with the highest confinement factor are used in the subsequent analysis. The modal intensity profiles for these two modes are nearly identical as the difference between the two is primarily in the phase (one modal field has in-phase lobes while the other has out-of-phase lobes). The coupling coefficient for the array is calculated using the modal effective index values for the two modes with highest modal confinement factors in accordance to Equations (2) and (3). This analysis is repeated for a variety of waveguide structures while varying design parameters to explore their effects on the modes and modal properties in the next section. The approximate index values used in our model are sufficient to demonstrate trends.

III. Design Parameter Sensitivity Analysis

Having modeled the supermodes of the 2-element VCSEL array, we can now do the same while varying the design parameters to explore the influence of design and choices on the modes and coupling. The parameters we will focus on will be the photonic crystal lattice period, the "fill-factor" (ratio of the etch-hole diameter to the lattice period), etch-hole index (presumed to be related to the depth of the photonic crystal etch), and index suppression in the cavity (presumed to be related to the injection current). Throughout this Section, we will take the array illustrated in Fig. 1 and defined by the parameters in Table I and perturb it by varying a single design parameter. Moreover, we depict the trends of each parameter using the same minimum/maximum plot scale for each figure.

A. Photonic Crystal Lattice Period

First, we consider in Fig. 3 the effects of increasing the photonic crystal lattice period. Analyzing the confinement factors for the two modes under investigation reveals that increasing the period increases the confinement but decreases the difference in confinement factor and thus the modal discrimination between the two modes as illustrated in Fig. 3. This is expected as increasing the lattice period increases the cavity diameter, and increasing waveguide size tends to decrease the modal discrimination.

Analyzing the complex coupling coefficient for the supermodes, plotted in Fig. 4, we find that both the real and complex terms show a decreasing trend as the period is increased. As

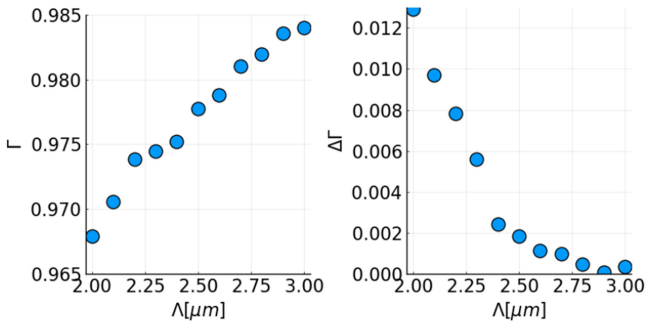

(a) Modal confinement factor (b) Difference in modal confinement factors

Fig. 3. The maximal modal confinement and the confinement factor difference as a function of lattice period.

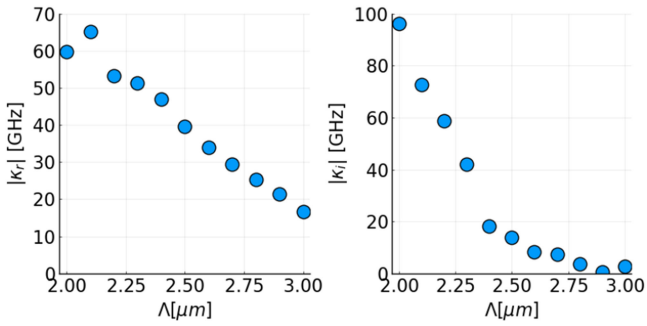

(a) Real coupling coefficient (b) Imaginary coupling coefficient

Fig. 4. The magnitude of the coupling coefficient terms as a function of lattice period.

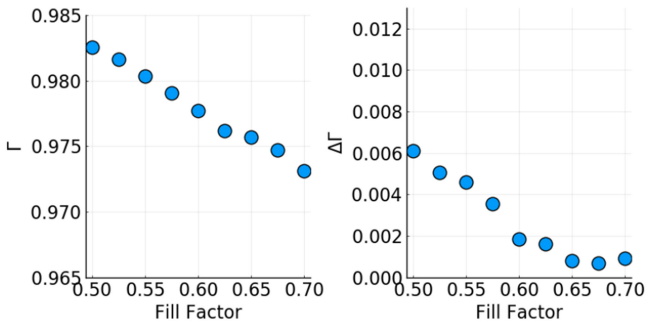

(a) Modal confinement factor (b) Difference in modal confinement factors

Fig. 5. The maximal modal confinement and the confinement factor difference as a function of photonic crystal fill-factor.

the imaginary component is related to the degree of modal discrimination between the modes, we can expect the decreasing trend with increasing period. Increasing the period and thus separation between cavities will tend to shift modal effective indices closer in value to each other, explaining the trend in the real component in Fig. 4(a).

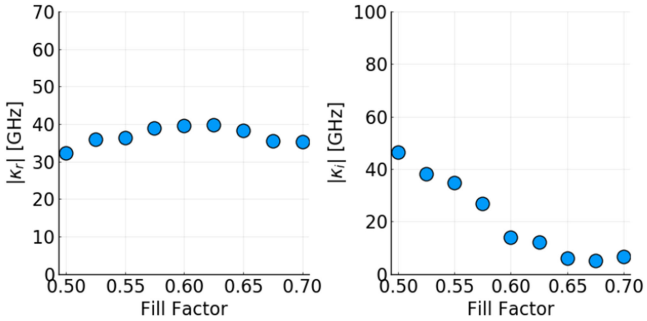

(a) Real coupling coefficient (b) Imaginary coupling coefficient

Fig. 6. The magnitude of the coupling coefficient terms as a function of photonic crystal fill-factor.

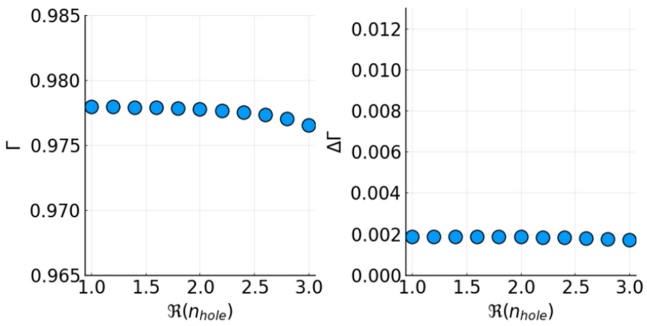

(a) Modal confinement factor (b) Difference in modal confinement factors

Fig. 7. The maximal modal confinement and the confinement factor difference as a function of hole index value (etch depth).

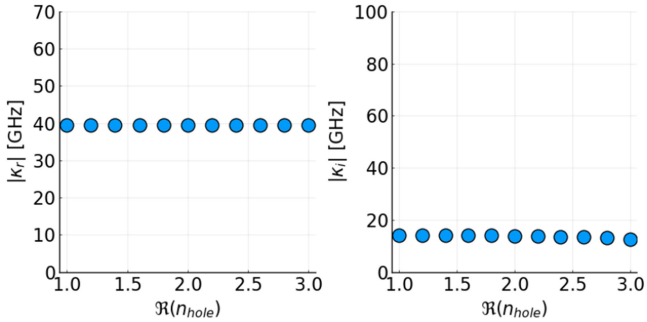

(a) Real coupling coefficient (b) Imaginary coupling coefficient

Fig. 8. The magnitude of the coupling coefficient terms as a function of hole index value (etch depth).

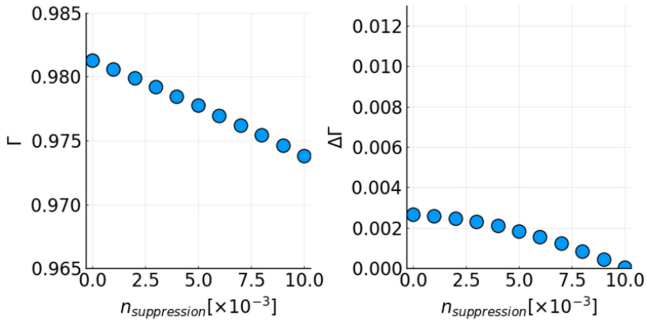

(a) Modal confinement factor (b) Difference in modal confinement factors

Fig. 9. The maximal modal confinement and the confinement factor difference as a function of cavity index suppression.

B. Photonic Crystal Fill-Factor

Fig. 5 depicts how the fill-factor influences the VCSEL array properties. Fig. 5(a) shows that increasing the fill-factor tends to decrease the confinement factor, as expected as increasing the fill-factor increases the etch-hole size and decreases the cavity size. The modal discrimination term shows slightly more complicated behavior, as the confinement factor difference decreases with increasing fill-factor until a fill-factor of 0.675, at which point it starts to increase. Note the overall variation is relatively minor in Fig. 5(b) compared to Fig. 3(b).

Fig. 6 reveals that neither the real or imaginary component of the coupling coefficient for the two supermodes exhibits monotonic relation with the photonic crystal fill-factor. The real component appears to increase the closer the fill-factor is to 0.625, and the imaginary component appears to decrease the closer it is to a fill-factor of 0.675.

C. Photonic Crystal Hole Etch

The photonic crystal hole index shows simpler intuitive trends, as illustrated in Fig. 7. Lowering the hole index effectively lowers the effective index of the waveguide, increasing the transverse optical confinement. This is in agreement with previous analysis of single element photonic crystal VCSELs [20]. The modal discrimination between the two array modes seems to have a similar dependence on the hole index, with lowered hole index increasing the difference in modal confinement factors. However, the degree of variation is very small in comparison to the variation due to either lattice period or fill-factor.

The hole index however, has very little influence on the coupling coefficients (Fig. 8).

D. Cavity Index Suppression

The influence of the cavity index suppression on confinement and confinement difference is depicted in Fig. 9. Increasing the index suppression in each element increases the antiguiding nature of the cavity, lowering the confinement factor and modal discrimination, albeit with moderate effect for both.

Varying the cavity index suppression also creates opposite trends in the real and imaginary components of the coupling coefficient, as seen in Fig. 10. Increasing the index suppression increases the real component and decreases the imaginary component.

E. Correlation Analysis

The previous sensitivity analysis was focused on single variable perturbations to a presumed "typical" waveguide structure. However, these design parameters may have similar trends across the larger, higher dimensional design space. To explore this, we randomly generate a set of 200 waveguide structures

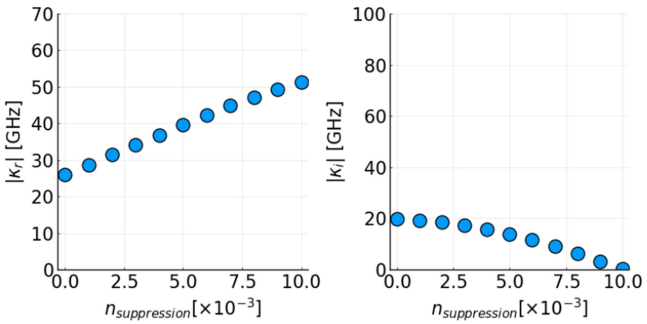

(a) Real coupling coefficient (b) Imaginary coupling coefficient

Fig. 10. The magnitude of the coupling coefficient terms as a function of cavity index suppression.

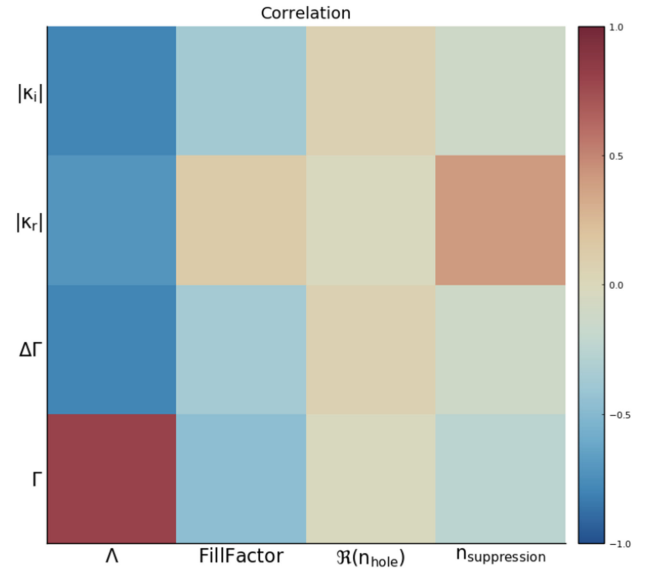

Fig. 11. Correlation coefficient between design parameters and modal properties.

within the larger design space (where each of the previously varied parameters is uniformly sampled over the same range of values used in the preceding analysis, namely $2 \leq \Lambda \leq 3\,\mu$m, $0.5 \leq$ FF ≤ 0.7, $1 \leq \Re(n_{\text{hole}}) \leq 3$, and $0 \leq n_{\text{suppression}} \leq 10^{-2}$) and calculate the modal properties as previously discussed. We can then calculate the (Pearson) sample correlation coefficients between the design parameters and modal performance parameters for this set of simulations. The correlation coefficient between a pair of variables X, Y is [23]:

$$\text{Cor}(X,Y) = \frac{\sum_i (x_i - \bar{x})(y_i - \bar{y})}{\sqrt{\sum_i (x_i - \bar{x})^2}\sqrt{\sum_i (y_i - \bar{y})^2}} \tag{4}$$

The linear correlation analysis comes with numerous limitations, namely weak correlation does not preclude non-linear relationships (such as those in Fig. 6) or mixed-variable relations. However, strong correlation (correlation magnitude values near one) should be indicative of a general trend [23].

Fig. 11 illustrates the coefficient of correlation between all of the array design parameters that are analyzed (photonic crystal period, fill-factor, etch hole index, and cavity index suppression) and the resulting supermode performance metrics (confinement factor, confinement factor difference, and the real and imaginary components of the coupling coefficient). The key takeaways from this analysis are that the photonic crystal period shows a strong positive correlation with the confinement factor and strong negative correlation with confinement factor difference and magnitude of the real and imaginary coupling coefficient. The photonic crystal fill-factor shows a weak positive correlation with the real coupling coefficients, and weak negative correlation with the confinement factor, confinement factor difference, and real coupling coefficient. The etch hole index and index suppression show minimal correlation with most of the supermode metrics, except for index suppression which shows moderate positive correlation with the real coupling coefficient.

We can try to fit a polynomial model to estimate the coupling coefficient values as functions of the design parameters under study. Using mixed selection of variables [23] where we iteratively select a set of polynomial terms below a certain order (eg 2 or 3) that give the greatest improvement in R^2 and remove terms as they become insignificant based on the t-value, we find that we can estimate the imaginary component of the coupling coefficient for the random structure modeling dataset. A simple model using using only the photonic crystal period and fill-factor, $|\kappa_i| \sim -1.9 \times 10^{12} + 1.0 \times 10^{12}\Lambda + 1.5 \times 10^{12}$FF $-5.2 \times 10^{11}\Lambda$FF $- 1.3 \times 10^{11}\Lambda^2$ (where κ_i is in Hz and Λ in micrometers), will fit the modeling dataset with $R^2 \approx 0.94$ (R^2 is the coefficient of determination, for which a value of 0 indicates model is no better predictor than the average value and a value of 1 indicates perfect model). We can similarly model the real component of the coupling coefficient, but now including the index suppression, to get $|\kappa_r| \sim -5.7 \times 10^{11} + 2.8 \times 10^{11}\Lambda + 2.1 \times 10^{13}\Delta n + 1.1 \times 10^{12}$FF $- 7.2 \times 10^{12}\Delta n\Lambda - 4.1 \times 10^{11}\Lambda$FF, with $R^2 \approx 0.95$.

IV. Conclusion

We have modeled 2×1 photonic crystal VCSEL arrays and calculated the array supermodes in order to analyze the effects of the array design parameters on the complex coupling coefficient. Although our models are not predictive of absolute coupling coefficient values, the sensitivity analysis determines which parameters are important for VCSEL array designs. Modifying the geometric parameters of the photonic crystal lattice, such as the lattice period or etch hole fill-factor, have the strongest effect on the coupling coefficient. Parameters related to refractive index, such as the etch hole index (related to etch depth) or cavity index suppression (related to carrier injection) have relatively smaller influence on the coupling coefficient, with the hole index having the weakest influence. As the lattice period and fill-factor vary, the real and imaginary components of the complex coupling coefficient also vary but with differing trends and thus should enable separate engineering of the real and imaginary components of the coupling coefficient. Future work to refine our model with comparison to experimental measurements will enable further tailoring of the array parameters to engineer desired optical or dynamical properties.

REFERENCES

[1] S. T. M. Fryslie, M. P. T. Siriani, D. F. Siriani, M. T. Johnson, and K. D. Choquette, "37-GHz modulation via resonance tuning in single-mode coherent vertical-cavity laser arrays," *IEEE Photon. Technol. Lett.*, vol. 27, no. 4, pp. 415–418, Feb. 2015, doi: 10.1109/lpt.2014.2376959.

[2] S. T. M. Fryslie *et al.*, "Modulation of coherently coupled phased photonic crystal vertical cavity laser arrays," *IEEE J. Sel. Topics Quantum Electron.*, vol. 23, no. 6, Nov./Dec. 2017, Art. no. 1700409, doi: 10.1109/jstqe.2017.2699630.

[3] H. Dave *et al.*, "Digital modulation of coherently-coupled 2 × 1 vertical-cavity surface-emitting laser arrays," *IEEE Photon. Technol. Lett.*, vol. 31, no. 2, pp. 173–176, Jan. 2019, doi: 10.1109/lpt.2018.2888806.

[4] H. Dave, Z. Gao, S. T. M. Fryslie, B. J. Thompson, and K. D. Choquette, "Static and dynamic properties of coherently-coupled photonic-crystal vertical-cavity surface-emitting laser arrays," *IEEE J. Sel. Topics Quantum Electron.*, vol. 25, no. 6, Nov./Dec. 2019, Art. no. 1700208, doi: 10.1109/jstqe.2019.2917551.

[5] Z. Gao, S. T. M. Fryslie, B. J. Thompson, P. S. Carney, and K. D. Choquette, "Parity-time symmetry in coherently coupled vertical cavity laser arrays," *Optica*, vol. 4, no. 3, pp. 323–329, Feb. 2017, doi: 10.1364/optica.4.000323.

[6] M. T. Johnson, D. F. Siriani, M. P. Tan, and K. D. Choquette, "Beam steering via resonance detuning in coherently coupled vertical cavity laser arrays," *Appl. Phys. Lett.*, vol. 103, no. 20, Nov. 2013, Art. no. 201115, doi: 10.1063/1.4830432.

[7] Z. Gao, B. J. Thompson, H. Dave, S. T. M. Fryslie, and K. D. Choquette, "Non-hermiticity and exceptional points in coherently coupled vertical cavity laser diode arrays," *Appl. Phys. Lett.*, vol. 114, no. 6, Feb. 2019, Art. no. 061103, doi: 10.1063/1.5083084.

[8] Z. Gao, B. J. Thompson, H. Dave, and K. D. Choquette, "The complex coupling coefficient of coherent VCSEL arrays," in *Proc. IEEE Int. Semicond. Laser Conf.*, Sep. 2018, pp. 1–2, doi: 10.1109/islc.2018.8516184.

[9] E. Kapon, A. Hardy, and A. Katzir, "The effect of complex coupling coefficients on distributed feedback lasers," *IEEE J. Quantum Electron.*, vol. QE-18, no. 1, pp. 66–71, Jan. 1982, doi: 10.1109/jqe.1982.1071364.

[10] H.-J. Yoo, J. R. Hayes, and Y.-S. Kwon, "Analysis of coupling coefficient between two vertical cavity surface emitting lasers for two-dimensional phase-locked array," *Electron. Lett.*, vol. 26, no. 13, pp. 896–897, 1990, doi: 10.1049/el:19900585.

[11] J. Katz, E. Kapon, C. Lindsey, S. Margalit, and A. Yariv, "Coupling coefficient of gain-guided lasers," *Appl. Opt.*, vol. 23, no. 14, pp. 2231–2233, Jul. 1984, doi: 10.1364/ao.23.002231.

[12] E. Kapon, J. Katz, and A. Yariv, "Supermode analysis of phase-locked arrays of semiconductor lasers," *Opt. Lett.*, vol. 9, no. 4, pp. 125–127, Apr. 1984, doi: 10.1364/ol.9.000125.

[13] Z. Gao, D. Siriani, and K. D. Choquette, "Coupling coefficient in antiguided coupling: Magnitude and sign control," *J. Opt. Soc. Amer. B*, vol. 35, no. 2, pp. 417–422, Jan. 2018, doi: 10.1364/josab.35.000417.

[14] Z. Gao, " Non-hermitian aspects of coherently coupled vertical cavity laser arrays," Ph.D. dissertation, Univ. Illinois at Urbana-Champaign, Aug. 2018. [Online]. Available: http://hdl.handle.net/2142/101491

[15] H. Dave, Z. Gao, and K. D. Choquette, "Complex coupling coefficient in laterally coupled microcavity laser diode arrays," *Appl. Phys. Lett.*, vol. 117, no. 4, Jul. 2020, Art. no. 041106, doi: 10.1063/5.0014468.

[16] Z. Gao, M. T. Johnson, and K. D. Choquette, "Rate equation analysis and non-hermiticity in coupled semiconductor laser arrays," *J. Appl. Phys.*, vol. 123, no. 17, May 2018, Art. no. 173102, doi: 10.1063/1.5022044.

[17] H. Dave, "Enhanced digital modulation of coherently coupled vertical cavity laser arrays: Theory and application," Ph.D. dissertation, Univ. Illinois at Urbana-Champaign, May 2019. [Online]. Available: http://hdl.handle.net/2142/107925

[18] L. A. Coldren, S. W. Corzine, and M. L. Mašanović, *Diode Lasers and Photonic Integrated Circuits*. Wiley, New York, USA, Mar. 2012, doi: 10.1002/9781118148167.

[19] K. Papatryfonos *et al.*, "Refractive indices of MBE-grown AlxGa(1-x)as ternary alloys in the transparent wavelength region," *AIP Adv.*, vol. 11, no. 2, Feb. 2021, Art. no. 025327, doi: 10.1063/5.0039631.

[20] D. F. Siriani, P. O. Leisher, and K. D. Choquette, "Loss-induced confinement in photonic crystal vertical-cavity surface-emitting lasers," *IEEE J. Quantum Electron.*, vol. 45, no. 7, pp. 762–768, Jul. 2009, doi: 10.1109/jqe.2009.2013124.

[21] D. F. Siriani and K. D. Choquette, "Implant defined anti-guided vertical-cavity surface-emitting laser arrays," *IEEE J. Quantum Electron.*, vol. 47, no. 2, pp. 160–164, Feb. 2011, doi: 10.1109/jqe.2010.2068278.

[22] B. J. Thompson, Z. Gao, S. T. M. Fryslie, and K. D. Choquette, "Mode engineering in linear coherently coupled vertical-cavity surface-emitting laser arrays," *IEEE J. Sel. Topics Quantum Electron.*, vol. 25, no. 6, Nov./Dec. 2019, Art. no. 1701205, doi: 10.1109/jstqe.2019.2950799.

[23] G. James, D. Witten, T. Hastie, and R. Tibshirani, *An Introduction to Statistical Learning*. New York, NY, USA: Springer, 2013, doi: 10.1007/978-1-4614-7138-7.

Pawel Strzebonski received the B.S. degree in 2016 in electrical engineering and the M.S. degree in electrical and computer engineering in 2018 from the University of Illinois, Urbana-Champaign, Urbana, IL, USA, where he is currently working toward the Ph.D. degree in electrical and computer engineering. His main research interests include computational methods for the design and characterization of various photonic devices, including photonic crystal VCSEL arrays and photonic crystal surface emitting lasers.

Kent D. Choquette (Fellow, IEEE) received the B.S. degrees from the University of Colorado Boulder, Boulder, CO, USA, and the M.S. and Ph.D. degrees in materials science from the University of Wisconsin-Madison, Madison, WI, USA. He held a Postdoctoral appointment with AT&T Bell Laboratories, Murray Hill, NJ, USA, and then joined Sandia National Laboratories, Albuquerque, NM, USA. In 2000, he joined the Electrical and Computer Engineering Department, University of Illinois at Urbana-Champaign, Champaign, IL, USA, and is currently the Able Bliss Professor of engineering. He leads the Photonic Device Research Group, which pursues the design, fabrication, characterization, and applications of semiconductor vertical-cavity surface-emitting lasers, photonic crystal light sources, nanofabrication technologies, and hybrid integration techniques. He has authored more than 300 technical publications and five book chapters, and presented numerous invited talks and tutorials at international conferences.

From 2000 to 2002, he was an IEEE Photonics Society Distinguished Lecturer. He is a Fellow of the Optical Society, SPIE, and American Association for the Advancement of Science. He is the Past President of the IEEE Photonics Society. Dr. Choquette was the recipient of the 2016 SPIE Technology Achievement Award, the 2012 OSA Nick Holonyak Jr. Award, and the 2008 IEEE Photonics Society Engineering Achievement Award.